nature materials

REVIEW ARTICLE

PUBLISHED ONLINE: 23 NOVEMBER 2011 | DOI: 10.1038/NMAT3151

Plasmonic-metal nanostructures for efficient conversion of solar to chemical energy

Suljo Linic*, Phillip Christopher and David B. Ingram

Recent years have seen a renewed interest in the harvesting and conversion of solar energy. Among various technologies, the direct conversion of solar to chemical energy using photocatalysts has received significant attention. Although heterogeneous photocatalysts are almost exclusively semiconductors, it has been demonstrated recently that plasmonic nanostructures of noble metals (mainly silver and gold) also show significant promise. Here we review recent progress in using plasmonic metallic nanostructures in the field of photocatalysis. We focus on plasmon-enhanced water splitting on composite photocatalysts containing semiconductor and plasmonic-metal building blocks, and recently reported plasmon-mediated photocatalytic reactions on plasmonic nanostructures of noble metals. We also discuss the areas where major advancements are needed to move the field of plasmon-mediated photocatalysis forward.

Plasmonic metallic nanostructures are characterized by their strong interaction with resonant photons through an excitation of surface plasmon resonance (SPR). SPR can be described as the resonant photon-induced collective oscillation of valence electrons, established when the frequency of photons matches the natural frequency of surface electrons oscillating against the restoring force of positive nuclei. The resonant photon wavelength is different for different metals. For example, gold, silver and copper nanostructures exhibit resonant behaviour when interacting with ultraviolet (UV) and visible (vis) photons (Fig. 1a). Because a large fraction of the abundant solar flux consists of UV–vis photons, these noble metals are of particular interest. The resonant wavelength and SPR intensity depend not only on the nature of the metal, but also on the size and shape of metallic nanostructures[1–4]. By manipulating the composition, shape and size (Fig. 1a–c, respectively) of plasmonic nanoparticles, it is possible to design nanostructures that interact with the entire solar spectrum and beyond[5,6].

As shown in Fig. 1, SPR is characterized by a build-up of intense, spatially non-homogeneous oscillating electric fields in the neighbourhood of the nanostructure[1–4]. SPR essentially acts to concentrate the light flux (the energy of incoming photons) in small volumes surrounding the nanostructure. Enhancements in the intensity of electric fields compared with the field intensity of the incoming photon flux are anywhere from $\sim 10^3$ at the surface of an isolated particle (Fig. 1d,e) to more than 10^6 for two particles separated by ~1 nm (Fig. 1f,g)[7,8]. The spots between plasmonic nanostructures with very high-intensity fields are often referred to as hot spots. Surface plasmons decay by either a radiative scattering of resonant photons, which is a characteristic of larger plasmonic nanostructures (for Ag, >50 nm), or the formation of energetic charge carriers, characteristic of smaller particles (<30 nm)[2,9]. The energetic carriers can be transferred to the surroundings[10,11] or relax by locally heating the nanostructure[12,13].

The unique capacity of plasmonic nanostructures to concentrate electromagnetic fields, scatter electromagnetic radiation, or convert the energy of photons into heat makes them suitable for various applications. Plasmonic metals have been used in single-molecule spectroscopy[4,7,14,15], surface-enhanced Raman spectroscopy[4,7,14], molecular sensing and detection in biological systems[12], medicinal heat-induced selective tissue targeting[12], solar cells[16] and many others[17]. These applications take advantage of either plasmon-amplified light-molecule interactions or laser-induced, plasmon-mediated local heating of nanostructures, which triggers accelerated thermal processes in the neighbourhood of the nanostructure. Several excellent reviews describing these applications are available, and we do not discuss these topics[4,7,12,13].

In this Review, we discuss recently demonstrated applications of excited plasmonic nanostructures in the field of photon-driven chemical conversion. We focus on two examples: (1) Plasmonic-metal-induced enhancements in the rates of photocatalytic water splitting (and related oxygen- and hydrogen- evolution half-reactions) on composite plasmonic-metal/semiconductor photocatalysts; and (2) direct, energetic electron-driven photocatalysis on plasmonic nanostructures. We exclusively spotlight the examples where plasmonic nanostructures were used to channel the energy of low-intensity UV–vis photons (comparable to solar intensity) to drive chemical transformations, and avoid discussing those where high-intensity lasers were used to induce local heating of the nanostructures and thereby facilitate thermochemical reactions[18,19].

To provide a contextual backdrop for this Review, we begin by brief discussions of the water-splitting process on semiconductors, the system configurations most often used to study it, and the materials used for the process. This is followed by a discussion of water-splitting reactions on plasmonic-metal/semiconductor composite photocatalysts and the mechanisms by which metal SPR can affect the photocatalytic activity of nearby semiconductors. We finish by discussing photocatalysis on excited, plasmonic metals and the models that can describe these photocatalytic processes. Throughout the Review we attempt to identify the critical parameters governing the design of photocatalysts that contain plasmonic metals.

Photocatalysis on semiconductors

Photocatalysts for various chemical transformations induced by UV–vis light, including splitting of water, are almost exclusively semiconductors[20,21]. In these systems, a flux of photons is absorbed by a semiconductor, yielding high-energy charge carriers (electron (e^-)–hole (h^+) pairs) in the semiconductor. The charge carriers separate from each other and diffuse to catalytically active sites at the semiconductor/liquid interface where they drive chemical transformations. In photocatalytic water splitting, energetic holes are involved in the oxygen-evolution half-reaction

Department of Chemical Engineering, University of Michigan, Ann Arbor, Michigan 48109, USA. *e-mail: linic@umich.edu

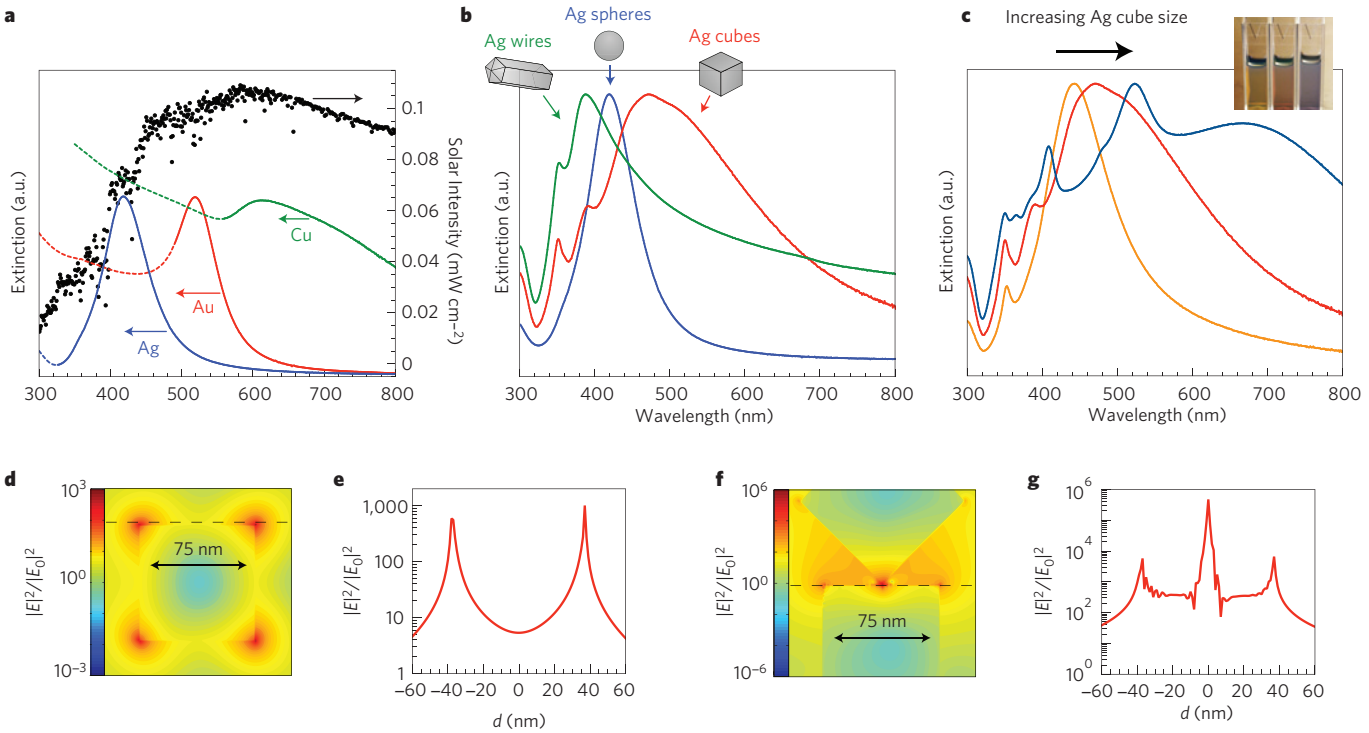

Figure 1 | Properties of plasmonic particles. a, Normalized extinction spectra of spherical Ag (38 ±12 nm diameter), Au (25 ±5 nm) and Cu (133 ±23 nm) particles. The intensity of solar radiation (data for air mass 1.5 solar spectrum from the National Renewable Energy Laboratory, http://rredc.nrel.gov/solar/spectra/am1.5/) is also shown, in black. The metal extinction is a consequence of the excitation of surface plasmon resonance. Dashed portions of the metal extinction curves indicate interband transitions (that is, no surface plasmon resonance in these regions). **b**, Normalized extinction spectra for Ag wire, cube and sphere nanoparticles. Wire-shaped particles are 90 ±12 nm diameter and >30 aspect ratio, cubic particles are 79 ±12 nm edge length and spherical particles are 38 ±12 nm diameter. **c**, Normalized extinction spectra for Ag nanocubes as a function of size (56 ±8 nm, 79 ±13 nm and 129 ±7 nm edge lengths correspond to orange, red and blue spectra respectively). The inset shows a photograph of the three nanocube samples suspended in ethanol. **d**, Spatial distribution of the SPR-induced enhancement of electric field intensity at the SPR peak wavelength (420 nm), from a FDTD simulation of a 75 nm Ag nanocube. **e**, Enhancement in the electric field intensity at the SPR peak wavelength as a function of distance, *d*, along the dashed line indicated in **d**. **f**, Spatial distribution of the SPR-induced enhancement of electric field intensity, from an FDTD simulation of two 75 nm Ag nanocubes separated by a distance of 1 nm (one cube is rotated 45°). **g**, Enhancement in the electric field intensity as a function of distance along the dashed line indicated in **f**.

(at low pH, $H_2O + 2h^+ \rightarrow 2H^+ + \frac{1}{2}O_2$), whereas energetic electrons participate in the hydrogen-evolution half-reaction (at low pH, $2H^+ + 2e^- \rightarrow H_2$)[22,23]. The net effect is that the energy of UV-vis photons is used to drive this highly endothermic chemical transformation, essentially depositing and storing solar energy into the energy of chemical bonds.

There are a number of system configurations that can be used to execute and/or study photocatalytic splitting of water[21–25]. One often-used design, initially introduced by Fujishima and Honda[22], employs a working semiconductor electrode deposited on a conductive substrate connected through an external circuit to a counter electrode. Introduction of light leads to the formation of electron–hole pairs in the semiconductor. For n-type (p-type) semiconductors, energetic holes (electrons) diffuse to the semiconductor/liquid interface where they participate in the oxygen- (hydrogen-) evolution half-reaction. Energetic electrons (holes) move to the counter electrode where they participate in the oxygen- (hydrogen-) evolution half-reaction. This photoelectrochemical cell design is particularly well suited for the investigations of the oxygen-evolution half-reaction on n-type semiconductors that by themselves do not evolve H_2 (Fig. 2a). In this design, Pt is typically used as a counter electrode for the hydrogen-evolution half-reaction, which does not require significant overpotential. An alternative design relies on photocatalysts that can perform both half-reactions on the surface of photocatalytic particles, shown in Fig. 2b. In these systems, both charge carriers (electron–hole pairs) diffuse to the surface of the semiconductor (more specifically, the interface of the semiconductor and reacting environment) where they drive the two half-reactions at the specifically designed sites, usually in the form of co-catalysts. The design of efficient photocatalysts that can execute both half-reactions has proved rather difficult. Thorough discussion of various configurations for water-splitting devices is available in a number of comprehensive reviews[21,23,25].

Although the appeal of the direct conversion of solar into chemical energy has been recognized for a long time, commercial applications of these technologies are scarce. As well as affordability and robustness, efficient photocatalysts need to: (1) absorb photons across the UV-vis region of the solar spectrum and convert these into electron–hole pairs; (2) allow for a facile separation of electron–hole pairs and their transport to the liquid/semiconductor junction where the half-reactions are performed; (3) have surface electronic structure tailored so that the half-reactions are thermodynamically feasible (product state in each half-reaction needs to have a lower free energy than the reactant state); and (4) possess high catalytic activity, that is, have surface sites that allow for the half-reactions to be performed with low activation barriers. Additional difficulties stem from the fact that the solar flux is a fairly diffuse energy source with ~100 mW (or ~10^{17} solar photons) impinging on the surface area of 1 cm^2 each second. This means that for a two-dimensional surface only ~100 solar photons interact with one surface atomic site (typical area of 10 $Å^2$) each second, establishing significant limitations on the maximum reaction rates.

These strict constraints have made it very difficult to identify promising water-splitting photocatalysts, as most single-component

materials do not satisfy all the requirements. For example, the most investigated n-type semiconductor photocatalyst, TiO_2, has a number of drawbacks including a large bandgap (~3.2 eV), which limits photo-absorption to only the UV region of the solar spectrum. As the UV region represents only ~5% of solar spectrum, TiO_2 is not efficient when sunlight is used to drive the reactions. Owing to its abundance and narrower bandgap than TiO_2, hematite (α-Fe_2O_3) is a promising photocatalyst for the oxygen-evolution half-reaction; however, it suffers from very low mobility of charge carriers and poor catalytic activity[26]. Semiconductors that exhibit excellent mobility of charge carriers, such as Si[27,28] and GaN[29] nanowires, in general exhibit fairly poor catalytic activities. More exhaustive reviews on the very active research area of semiconductor materials for water splitting are available[20,21,25].

Composite plasmonic-metal/semiconductor photocatalysts

It has previously been shown that some of the inherent problems of semiconductor photocatalysts can be alleviated by creating multifunctional co-catalyst/semiconductor photocatalysts. One class of these materials consists of co-catalyst nanoparticles (for example Ir (ref. 30), Pt (ref. 30), Au (refs 30–32), Ag (ref. 33), or various metal oxides) deposited directly on a semiconductor. The role of the co-catalyst is to perform the catalytic function by providing chemically active sites where relevant chemical transformations can take place with lower activation barriers than on the semiconductor. Furthermore, co-catalyst nanoparticles act to extend the lifetime of energetic charge carriers that reach the surface of the semiconductor by enhancing the rates of electron–hole separation at the co-catalyst/semiconductor interface. There are many reviews on these topics[10,34].

Although this co-catalyst/semiconductor class exhibits improved performance compared with semiconductor photocatalysts, this approach does not address the problems of: (1) very diffuse solar flux; (2) absorption limited to only high-energy photons in many inexpensive and abundant semiconductors (for example, TiO_2); and (3) large discrepancy in photon penetration depths (a few nanometres to micrometres) and minority charge-carrier diffusion length (a few nanometres) encountered by many promising semiconductors. The main consequence of this is that many energetic charge carriers are generated far from a reactive surface and recombine rather than participating in photocatalytic reactions. It has been recognized recently that these problems can be partially alleviated by formulating composite photocatalysts consisting of photo-excited plasmonic metallic nanostructures embedded in semiconductor matrices.

This was demonstrated in a number of studies that showed that composite plasmonic-metal/semiconductor photocatalysts achieved significantly higher rates in various photocatalytic reactions compared with their pure semiconductor counterparts[11,32,35–48]. For example, Fig. 3a shows that the rate of oxygen evolution under broadband visible illumination (>400 nm) of Sun-like intensity is significantly enhanced on composites of plasmonic Ag and N-doped TiO_2 (N–TiO_2) compared with pure Ag or N–TiO_2 (ref. 44). These studies were carried out in a photoelectrochemical cell with a Pt counter electrode for the hydrogen-evolution half-reaction. Similar conclusions, pointing to the superior photocatalytic activity of composite plasmonic-metal/semiconductor photocatalysts, were obtained by Cronin and co-workers who studied the oxygen-evolution half-reaction on TiO_2 and composites containing plasmonic Au nanostructures and TiO_2 under illuminations of 532 and 633 nm, shown in Fig. 3b[47]. Garcia and co-workers arrived at similar conclusions in their studies, which showed that the rate of hydrogen-evolution half-reaction was higher on plasmonic Au/TiO_2 composites than on TiO_2 under broadband visible illumination (>400 nm) of Sun-like intensity (Fig. 3c)[32]. In these studies methanol was used as an efficient scavenger of energetic holes generated in TiO_2 particles.

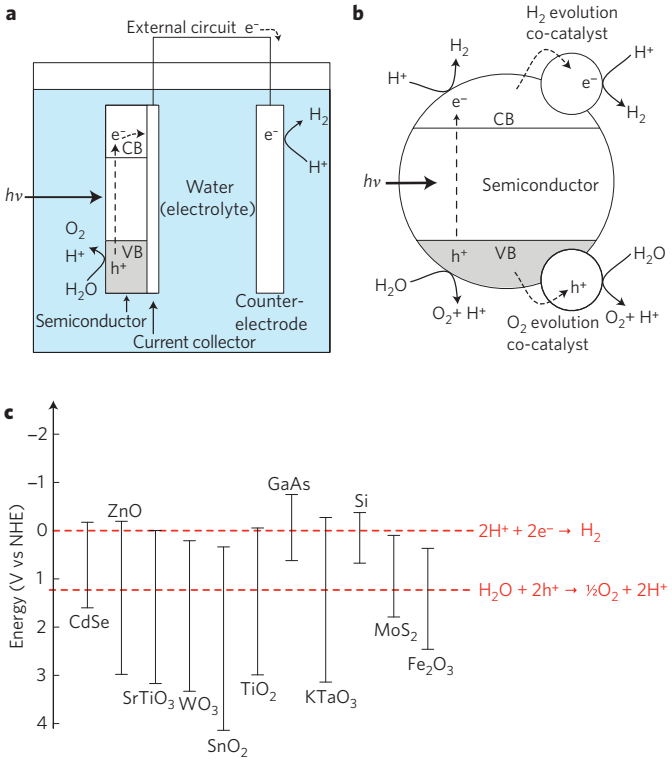

Figure 2 | Semiconductor photocatalysis. a, Photoelectrochemical cell design for water splitting (processes for an n-type semiconductor are shown). When illuminated with photons ($h\nu$) of energy exceeding the bandgap, excited charge carriers are formed in the semiconductor photoanode. The holes diffuse to the semiconductor surface and drive the oxygen-evolution half-reaction ($2H_2O + 4h^+ \rightarrow O_2 + 4H^+$). Electrons are collected and travel to the counter electrode where they drive the hydrogen-evolution half-reaction ($2H^+ + 2e^- \rightarrow H_2$). **b**, Particle-based water-splitting photocatalyst. Excited charge carriers (both electrons and holes) diffuse to the particle surface where they drive the two half-reactions, usually at specially designed co-catalyst sites. VB, valence band; CB, conduction band. **c**, VB and CB for a range of semiconductors (data from refs 90 and 91) on a potential scale (V) versus the normal hydrogen electrode (NHE). Redox potentials for the water-splitting half-reactions versus the NHE are also indicated by dashed red lines. For the water-splitting reaction to be thermodynamically favourable, the bandgap should straddle these redox potentials, that is, the CB should have higher energy (more negative potential) than the hydrogen-evolution potential and the VB should be lower in energy than the oxygen-evolution potential.

Role of metal SPR

A unique characteristic of composite photocatalysts that contain semiconductor and plasmonic-metal nanostructures is that plasmonic nanostructures interact with light through an excitation of SPR. Strong evidence that SPR played an important role in enhancing the rate of photocatalytic reactions on nearby semiconductors was obtained in the measurements of the rate enhancements induced by plasmonic metal as a function of excitation wavelengths. These measurements showed that for all studied reactions, including oxygen- and hydrogen-evolution half-reactions on numerous semiconductors, the highest rate enhancements were observed at the wavelengths corresponding to the metal SPR[11,38,39,43,44,46–48]. Identical conclusions were obtained in studies where the SPR intensity and wavelength were modulated by manipulating the composition, shape, or size of plasmonic nanostructures[36,44]. These studies conclusively demonstrated that a positive relationship exists between SPR intensity and the rate enhancements, and led to a hypothesis that the metallic SPR enhances rates of

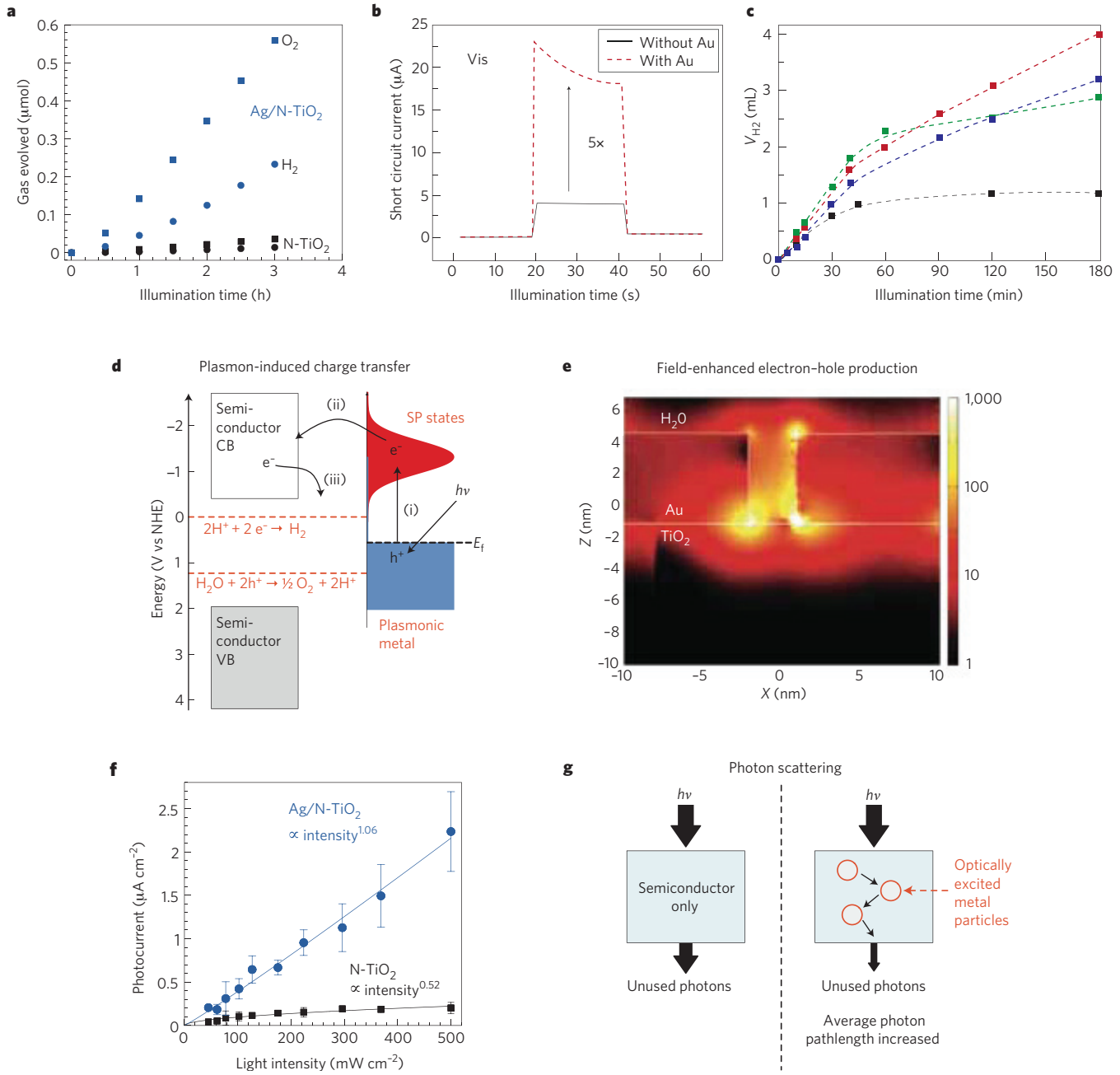

Figure 3 | Plasmon-enhanced semiconductor photocatalysis. a, Evolution of oxygen and hydrogen on N-TiO_2 and Ag/N-TiO_2 composite photoelectrodes under broadband visible illumination (>400 nm) of solar intensity[44]. The addition of photo-excited Ag nanoparticles enhances the rate of water splitting. **b**, Photocurrent (measure of the reaction rate) generated during oxygen evolution on 'anodic TiO_2' and Au/TiO_2 photoelectrodes under visible illumination (533 nm)[47]. The visible activity of the TiO_2 sample (without Au) was ascribed to impurity and defect states. **c**, The volume of evolved hydrogen, V_{H2}, on TiO_2 (black squares) and Au/TiO_2 composites with three different weight loadings of Au with respect to TiO_2 (red circles, 0.25% Au; green triangles, 1.5% Au; blue triangles, 2.2% Au) on illumination with a broadband visible light source (>400 nm)[32]. **d**, Mechanism of SPR-induced charge transfer with approximate energy levels on the NHE scale. Dashed red lines refer to the water-splitting redox potentials (see Fig. 2a). (i) Electrons near the metal Fermi level, E_f are excited to surface plasmon (SP) states; (ii) the electrons transfer to a nearby semiconductor particle; (iii) this activates electron-driven processes such as the hydrogen-evolution half-reaction. **e**, Optical simulations showing SPR-enhanced electric fields owing to photo-excited Au particles, permeating into a neighbouring TiO_2 structure[47]. The colour bar shows electric field intensity normalized by the light source intensity ($|E|^2/|E|_0^2$). The electric field intensity (and therefore charge-carrier generation) is the highest at the TPB. **f**, Photocurrent measured in the process of oxygen evolution as a function of broadband visible light intensity for N-TiO_2 and Ag/N-TiO_2 photo-electrodes[44]. The rate on TiO_2 photo-electrodes shows approximately a ½ order dependence on intensity, whereas for Ag/N-TiO_2 composites the rate varies linearly with light intensity. **g**, Schematic illustrating the scattering mechanism. The addition of optically excited plasmonic nanoparticles increases the average path length of photons in the composite structure. Figures reproduced with permission from: **a**,**b**,**c**,**e**,**f**, refs 44, 47, 32, 47, 44 respectively, © 2011 ACS.

photocatalytic reactions on nearby semiconductors by transferring energy to the semiconductor and increasing the steady-state concentration of 'chemically useful' energetic charge carriers in the semiconductor. We use the term 'chemically useful' to refer to the charge carriers at the surface of the semiconductor that participate in photocatalytic transformations.

There are three non-mutually exclusive energy-transfer mechanisms by which SPR can enhance the concentration of charge carriers, and therefore the rates of photocatalytic reactions, in a nearby semiconductor. We discuss these mechanisms below.

SPR-mediated charge injection from metal to semiconductor. In one of these mechanisms, charge carriers are directly injected from excited plasmonic-metal nanostructures into the semiconductor surface[11,32,37–39,41,43,48]. The charge injection mechanism is analogous to dye sensitization, where a dye molecule, anchored to a semiconductor, acts to absorb light and transfer energetic charge carriers to the semiconductor[24,49]. The metallic plasmonic nanoparticles essentially act as a dye sensitizer, absorbing resonant photons and transferring the energetic electron, formed in the process of the SPR excitation, to the nearby semiconductor (Fig. 3d). Because plasmonic nanostructures of noble metals are characterized by an excellent mobility of charge carriers and high absorption cross-sections, which are, under resonance conditions, up to 10^5 larger than the cross-section of typical dye-sensitizer molecules, they represent very promising sensitizers[50]. Furthermore, the ability to tune the resonance wavelength by changing the size or shape of nanostructures suggests that the entire solar spectrum can be exploited using the plasmonic-metal sensitizers.

The charge injection mechanism was found to be functional in composite photocatalysts where the plasmonic nanoparticles and semiconductor are in direct contact with each other, allowing a rapid transfer of charge carriers. These composite systems are geometrically similar to the conventional co-catalyst/semiconductor photocatalysts that are often synthesized by an incipient wetness deposition of metal precursors and their subsequent thermal treatment on a semiconductor surface. In these systems, the centres where a photoreaction can take place are at a metal/semiconductor/liquid three-phase boundary (TPB) and they spread away from the TPB along the semiconductor/liquid interface approximately the length of the characteristic semiconductor charge-carrier diffusion.

It is important to note that most semiconductors of interest for water splitting are characterized by their conduction bands somewhere between −1.0 and 0 V on the normal hydrogen electrode (NHE) scale (Fig. 2c). Their valence bands are between 2.0 and 3.5 V (electron energy between −2.0 and −3.5 eV) on the NHE scale. For nanoparticles of noble metals, the SPR energy is between 1.0 and 4.0 eV with respect to the metal Fermi level, and the energetic electron formed in the process of the SPR excitation will be in this energy window. The Fermi level for noble metals is around 0 V on the NHE scale. Owing to this alignment of the electronic states, in general the plasmonic-metal/semiconductor systems allow for the transfer of only energetic electrons from the metal to the semiconductor. As a consequence the charge injection mechanism should play a role in the systems where high-energy electrons are required to execute half-reactions on semiconductors, such as hydrogen-evolution reaction (Fig. 3d). It is worth mentioning that a few reports suggested that energetic holes retained on very small plasmonic-metal particles (particles of Au of ~2 nm diameter), have sufficient energy to drive the oxygen-evolution half-reaction on the surface of the metal[32,41].

Near-field electromagnetic and scattering mechanisms

SPR-induced enhancements in the photocatalytic activity of semiconductors were also observed on systems where the semiconductor and plasmonic metal were separated from each other by thin, non-conductive spacers preventing any direct charge exchange between the two building blocks[35,36,40,44]. In these systems, radiative energy transfer from the metal SPR to the semiconductor can take place through near-field electromagnetic and resonant photon-scattering mechanisms.

The near-field electromagnetic mechanism is based on the interaction of the semiconductor with the strong SPR-induced electric fields localized nearby at the metallic nanostructure. As shown in Fig. 1, photo-excited plasmonic nanostructures are characterized by strong electric fields that are orders of magnitude higher than the field of photons used to photo-excite the nanostructure. These fields are spatially non-homogenous, with the highest intensity at the surface of the nanostructure and decreasing exponentially with distance from the surface within ~20–30 nm and linearly further away. We note that significant fields are present even a few nanometres away from the nanostructure. When a semiconductor is brought into the proximity of a photo-excited plasmonic nanostructure it encounters these intense fields. As the rate of electron–hole formation in a semiconductor is proportional to the local intensity of the electric field (more specifically $|E|^2$) (refs 51,52), the rate of electron–hole formation in some regions of the semiconductor increases by a few orders of magnitude (Fig. 3e). Photo-excited plasmonic nanostructures essentially play a role of nanosized concentrators that can amplify the local light intensity. Another important consequence of spatially non-homogenous intense fields is that the rate of SPR-induced electron–hole pair formation is highest in the parts of the semiconductor closest to the plasmonic nanostructure, that is, near the surface (essentially at the semiconductor/liquid interface). The selective formation of charge carriers in the region of the semiconductor closest to the semiconductor/liquid interface rather than in the bulk of the semiconductor offers a few critical additional advantages: (1) they are readily separated from each other under the influence of the surface potential; and (2) they have a shorter distance to migrate to reach the semiconductor/liquid interface, where they can perform photocatalytic transformations. This effectively means that the probability of photoreaction is enhanced relative to the probability of charge-carrier recombination.

The dominant role of the near-field electromagnetic mechanism was suggested based on electrodynamic simulations, which showed that the rate of electron–hole formation in semiconductors was enhanced in the regions of proximity of the excited plasmonic nanostructure (Fig. 3e)[35,41,47]. The proposed mechanism was also recently supported in a set of chemical probe experiments where the rate of photoelectrocatalytic oxygen-evolution half-reaction was measured as a function of broadband light intensity on composites of plasmonic Ag nanostructures and N-doped TiO_2 (N-TiO_2) semiconductor and N-TiO_2-only electrodes. The composite photocatalysts contained a physical mixture of N-TiO_2 (~25 nm particles) and plasmonic Ag nanocubes (~120 nm edge length), separated from each other by thin, non-conductive spacers preventing any direct charge exchange between the two building blocks[44]. A Pt counter electrode was used for hydrogen-evolution half-reaction. As shown in Fig. 3f, a linear dependence of the reaction rate on light intensity was observed for the composite photoelectrodes, compared with ~½ order dependence for the semiconductor. It had been demonstrated previously that charge carriers formed in the TiO_2 bulk mainly relax through the process of direct electron–hole recombination, and that this decay mechanism results in a half-order dependence of the surface concentration of charge carriers on the intensity[53]. However, the charge carriers formed close to the surface of TiO_2 decay mainly in their reaction with surface trap states, and the surface concentration of charge carriers exhibits a first-order dependence on the source intensity[54]. Because the rate of the oxygen-evolution half-reaction is linearly proportional to the concentration of holes at the surface of the semiconductor, the observed linear intensity dependence of rate in the composite plasmonic-metal/semiconductor systems is an indication that charge carriers are selectively formed in the semiconductor close to the semiconductor/liquid interface.

In addition to the local electric fields, which play a role in the spatially non-homogeneous formation of electron–hole pairs in

nearby semiconductors, for large plasmonic nanostructures (larger than ~50 nm in diameter) the metal SPR is accompanied by an efficient scattering of resonant photons[2,9]. This scattering of photons by plasmonic nanostructures increases the average photon path length in plasmonic nanostructures and semiconductor composites, causing an increased rate of electron–hole pair formation in the semiconductor (Fig. 3g). Here, the plasmonic nanostructure essentially acts as a nanomirror, some resonant photons that are not absorbed by the semiconductor on first pass through the composite material could be scattered by the nanostructure, effectively giving those photons many passes through the system.

It is important to note that the mechanisms involving radiative energy transfer from excited plasmonic metal to nearby semiconductor (near-field electromagnetic and scattering mechanism) were further supported by measurements of semiconductor photoluminescence emission[36,51,55,56]. These studies showed that the rate of semiconductor emission (which is proportional to the concentration of electron–hole pairs in the semiconductor) for composite systems was larger than for semiconductor-only systems. Furthermore, it was shown that the enhancements in the emission were positively related to the intensity of metal SPR. The observed wavelength-dependent enhancements in the semiconductor emission can be explained only by the metal-SPR-induced increase in the rate of electron–hole formation in the nearby semiconductor[36,51,56].

Critical design parameters for composite photocatalysts

It is obvious that the magnitude of SPR-induced rate enhancements and the relative importance of the three mechanisms will be governed by the optical properties of metal and semiconductor building blocks and their geometric arrangements in the composite systems. For example, charge injection is the exclusive mechanism for composite photocatalysts where the metal SPR is of a lower energy than the semiconductor bandgap. In these systems, the metal SPR allows for an effective extension of absorption bands in the composite photocatalysts compared with the semiconductor. The near-field electromagnetic and scattering mechanisms are important for composite photocatalysts with an overlap between the spectra of the illumination source, metal nanoparticle SPR and semiconductor absorbance[57]. Essentially, the source photons need to excite SPR in the metal nanostructure and the resonant photons (or local electromagnetic fields) need to have sufficient energy to overcome the semiconductor bandgap.

As well as their optical properties, the relative geometric arrangement of semiconductor and metal building blocks has an important effect. If the building blocks are in direct contact, all three mechanisms could play a role, subject to the above discussed constraints associated with optical properties. For composites where the building blocks are separated from each other by non-conductive spacers, such as organic molecules[36,44] or porous inorganic films[35,40], the near-field and scattering mechanisms are functional. Composite systems where plasmonic nanostructures are positioned to allow for numerous passes of resonant photons through the semiconductor matrix will exhibit very strong scattering effects. However, the composite systems that are characterized by large plasmonic-metal/semiconductor interfacial areas should exhibit strong near-field effects.

Furthermore, the magnitude of rate enhancements owing to the near-field effect is also governed by the relative geometric arrangements of building blocks. The SPR-induced increase in the rate of electron–hole formation in a nearby absorber (the semiconductor in this case) through the near-field mechanism is dependent on the intensity of local fields. The field intensity is a strong function of the relative arrangement of plasmonic nanostructures (for an example see Fig. 4a) and the spacing between the photo-excited plasmonic metal and absorber[52,58,59]. Moreover, the presence of a metal surface close to the semiconductor can also decrease the lifetime of energetic charge carriers in the semiconductor by increasing the rates of radiative emission and non-radiative energy dissipation[51,56].

The impact of the spacing between semiconductor and plasmonic-metal building blocks on reaction rates was illustrated recently by measuring the rate enhancement in oxygen-evolution half-reaction as a function of the thickness of inorganic[40] and organic non-conductive spacers between the building blocks. Figure 4b shows unpublished results from our lab, in which the rate of the oxygen-evolution half-reaction on UV illumination (365 nm) was measured as a function of the distance between a non-porous TiO_2 film and excited plasmonic Ag nanoparticles deposited on the film. The separation distance between Ag and TiO_2 was controlled by applying non-conductive polymer (polyethylene glycol) films of different thickness between them. These measurements showed that the rate

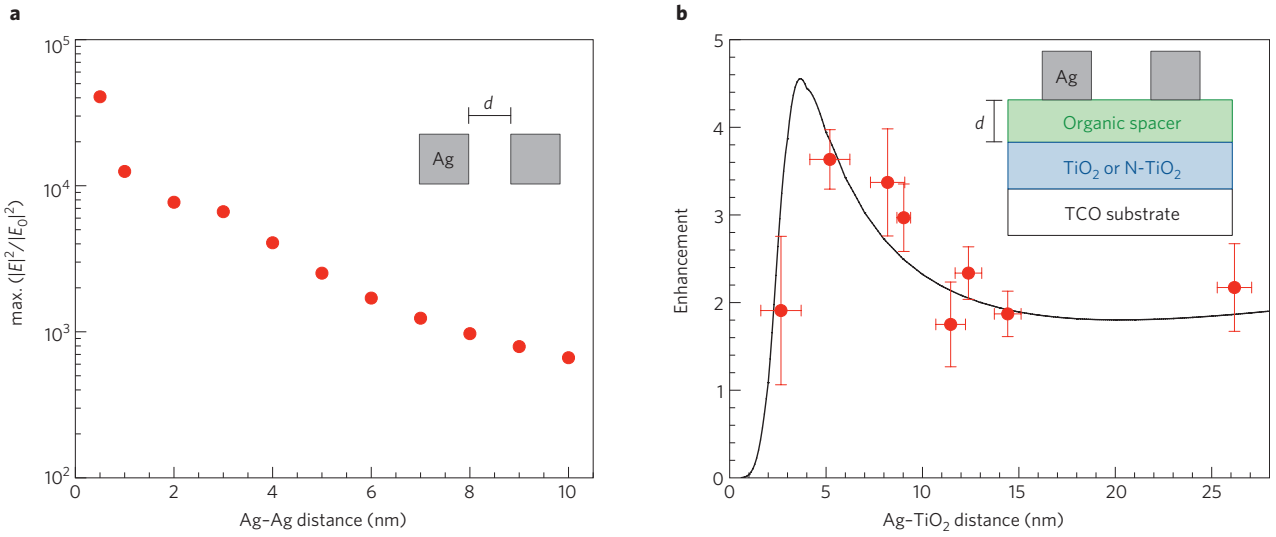

Figure 4 | Design considerations for plasmonic-metal/semiconductor composite photocatalysts. a, Maximum enhancement in the electric field intensity (E^2) as a function of distance between two Ag particles, calculated from a series of finite-difference time-domain simulations (S. Linic, P. Christopher and D. B. Ingram, unpublished observations). **b**, Photocurrent enhancement (proportional to oxygen-evolution rate) measured as a function of distance between Ag and TiO_2 building blocks (S.L., P.C. and D.B.I., unpublished observations). The distance was controlled by varying the thickness of an organic spacer layer (polyethylene glycol). The thickness was measured using ellipsometry. The black curve shows the results of a theoretical model discussed in the main text.

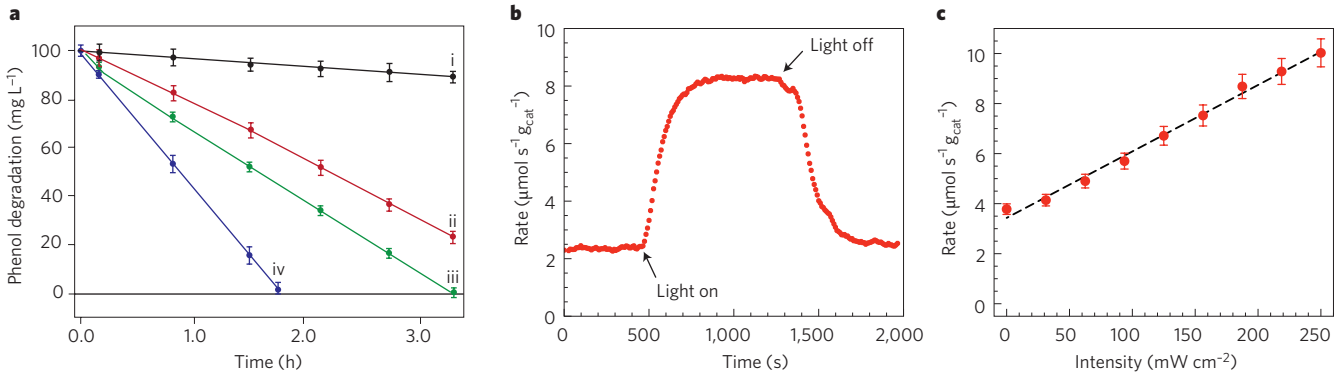

Figure 5 | Plasmon-enhanced photocatalysis on metal surfaces. a, The rate of phenol degradation by the Fenton reaction over catalysts composed of photo-excited plasmonic Ag nanoparticles supported on a modified diamond nanoparticle support[69]. The reactions were carried out in a batch reactor at 300 K and pH 4. Significant enhancements in the rate were observed on the introduction of light. The catalyst was illuminated using a pulsed laser (532 nm) at various source energies: (i) 0 mJ per pulse, (ii) 20 mJ per pulse, (iii) 38 mJ per pulse and (iv) 70 mJ per pulse. Furthermore, the reaction rate was linear with respect to source intensity, indicating that energetic electrons mediate the photocatalytic process. **b**, The rate of ethylene epoxidation at 450 K over catalysts consisting of plasmonic Ag nanocubes with 60 nm edge length supported on α-Al_2O_3 (ref. 70). A significant enhancement in the rate is observed when light is introduced. The illumination source was a broadband visible light with an intensity of 250 mW cm^{-2} and peak wavelength of 590 nm. **c**, The rate of photothermal (light on) ethylene epoxidation over Ag nanocube/Al_2O_3 catalyst as a function of source intensity[70]. The measurements were performed at a constant temperature of 470 K. The linear relationship (dashed line) between the rate and intensity is a signature of an electron-driven catalytic process. Figures reproduced with permission from: **a**, ref. 69, © 2011 ACS; **b**,**c**, ref. 70, © 2011 NPG.

enhancement is highest at a separation distance of ~2–6 nm between the building blocks. Figure 4b also shows that the dependence of the rate enhancement as a function of the distance between the building blocks can be quantitatively captured by a simple model designed to quantify the relative concentration of charge carriers at the semiconductor surface. The model assumes that the increase in the rate of charge-carrier formation in a semiconductor can be described, as discussed above, in terms of the plasmon-induced electric-field enhancement, which exponentially decreases with distance from the surface within ~20–30 nm and linearly further away. However, the efficiency of metal-stimulated non-radiative energy dissipation, η, which is the main channel for the loss of energetic charge carriers in the semiconductor owing to the presence of the metal surface, can be approximated by the Förster resonant energy transfer (FRET) equation, $\eta = R_0^6/(R_0^6 + d^6)$, where d is the distance between building blocks and R_0 is the Förster radius (the separation distance yielding 50% FRET efficiency)[60,61]. R_0 can be calculated and typically has a value of approximately 5 nm (ref. 61). At the limit of infinite separation between the plasmonic metal and semiconductor, the local field enhancement is small and the rate of charge-carrier formation is low (the enhancement is only a result of the scattering mechanism). However, at the limit of very small separation, the efficiency of FRET loss is very high and most charge carriers are lost in the non-radiative FRET process. The optimal distance is obtained as a compromise between these two extremes, which is in general attained for the distance of a few nanometres between the building blocks.

The contributions discussed above have conclusively established that excited plasmonic nanostructures enhance the rates of photocatalytic reactions, including those associated with the solar splitting of water, on nearby semiconductors. Three different mechanisms for the SPR-mediated rate enhancements have been outlined and the impact of optical and geometric properties of composite photocatalysts on their performance has been analysed.

Another potentially promising use of plasmonic nanostructures in the field of chemical conversion centres on recently demonstrated direct SPR-driven photocatalysis on excited plasmonic metal nanostructures. The examples of this phenomenon have so far been limited to just a few exothermic reactions. It was demonstrated that the main role of metal SPR was to accelerate the overall rate of the chemical transformations at a given temperature. We discuss these processes in the next section.

Photocatalysis on plasmonic nanostructures

Although metals have high inherent chemical activity and ability to selectively activate numerous chemical transformations, it has been recognized that the rates of photocatalytic reactions on metals at Sun-like photon intensities are very low owing to low efficiencies of energetic charge-carrier formation and short lifetimes[62–67]. It was shown recently that unlike other metal structures, photo-excited plasmonic nanostructures exhibit relatively high photocatalytic activity when exposed to resonant photons of Sun-like intensities[68–73]. The observations of the direct photocatalysis of plasmonic nanostructures have so far been limited only to a number of exothermic partial oxidation, selective reduction, and organic decomposition reactions on excited plasmonic Ag and Au nanostructures. In Fig. 5 we summarize some of the reported results and elaborate on experimental set-ups.

Mechanism of photocatalysis on excited plasmonic metals. Although the number of detailed experimental studies of these systems is rather limited, we will briefly summarize the main findings of the analyses performed so far and discuss the molecular model for these reactions. An analysis of gas-phase partial oxidation reactions on excited plasmonic Ag nanostructures established that, at a constant temperature, the reaction rates exhibited strong dependence on the light wavelength, peaking at the wavelengths where the plasmon intensity was the highest[70]. These measurements provided a clear indication that the excitation of surface plasmons was responsible for the observed photocatalytic activity. It was also demonstrated that these reactions exhibited distinct signatures of energetic electron-induced chemical reactions on metals (that is, the reactions initiated by transfer of high-energy electrons from the metal to the reactant), including: (1) the linear dependence of the reaction rate on light intensity[69,71,74]; (2) larger kinetic isotope effects compared with the reaction driven using only thermal energy source (that is, the phonon-driven counterparts)[70,75,76]; and (3) different product selectivity for the reactions induced by the thermal flux compared with the same chemical transformation induced by a photon source[68,69]. Based on experimental and first-principles computational studies, it was proposed that SPR acts to donate energetic electrons into available adsorbate (reactant) states (orbitals), forming a negative ion species. This process is very similar to the above-discussed SPR-mediated charge injection from an excited plasmonic

metal to a nearby semiconductor, except that the charge is injected in adsorbate states rather than in a semiconductor conduction band. We note that the formation of charged ion adsorbates could also be initiated by photon-induced interband transition in metals; however, for noble metals these transitions take place at UV photon wavelengths (that is, they are blue shifted compared with SPR). In fact, there have been a few reports of photocatalytic oxidation reactions on Au and Ag catalysts, under UV illumination, that have been explained in the context of interband transitions on metals[68,72,73].

The negative ion formed in the process of electron transfer from metal to adsorbate can, depending on its potential energy landscape, undergo a rapid reaction on the metal surface[70] or it can move to the solution where it reacts[69,72,73]. The negative ion that rapidly reacts on the metal surface is often referred to as the transient negative ion (TNI)[75–81]. Figure 6 contains a more detailed discussion of the formation and subsequent relaxation of the O_2^- TNI on the surface of plasmonic Ag, leading to the dissociation of O_2. It is worth noting that the probability for the formation of the negative ion and its subsequent reaction on the metal surface can be captured by well-developed models for reactions induced by electronic transitions and reactions induced by multiple electronic transitions[78–81]. As these models were first used to describe electron-induced desorption on metals, they are better known as desorption induced by electronic transition (DIET) and desorption induced by multiple electronic transitions (DIMET). Excellent reviews discussing these mechanisms have been written[62,82–84]. DIET and DIMET analysis showed that the probability for SPR-induced electron-driven transformations on metals is affected by many factors including the availability of low-lying molecular orbitals on the adsorbate, the potential energy landscape for the charged and neutral adsorbates, the lifetime of the charged adsorbate state, the surface-plasmon intensity, and the temperature of the plasmonic nanostructures (Fig. 6c).

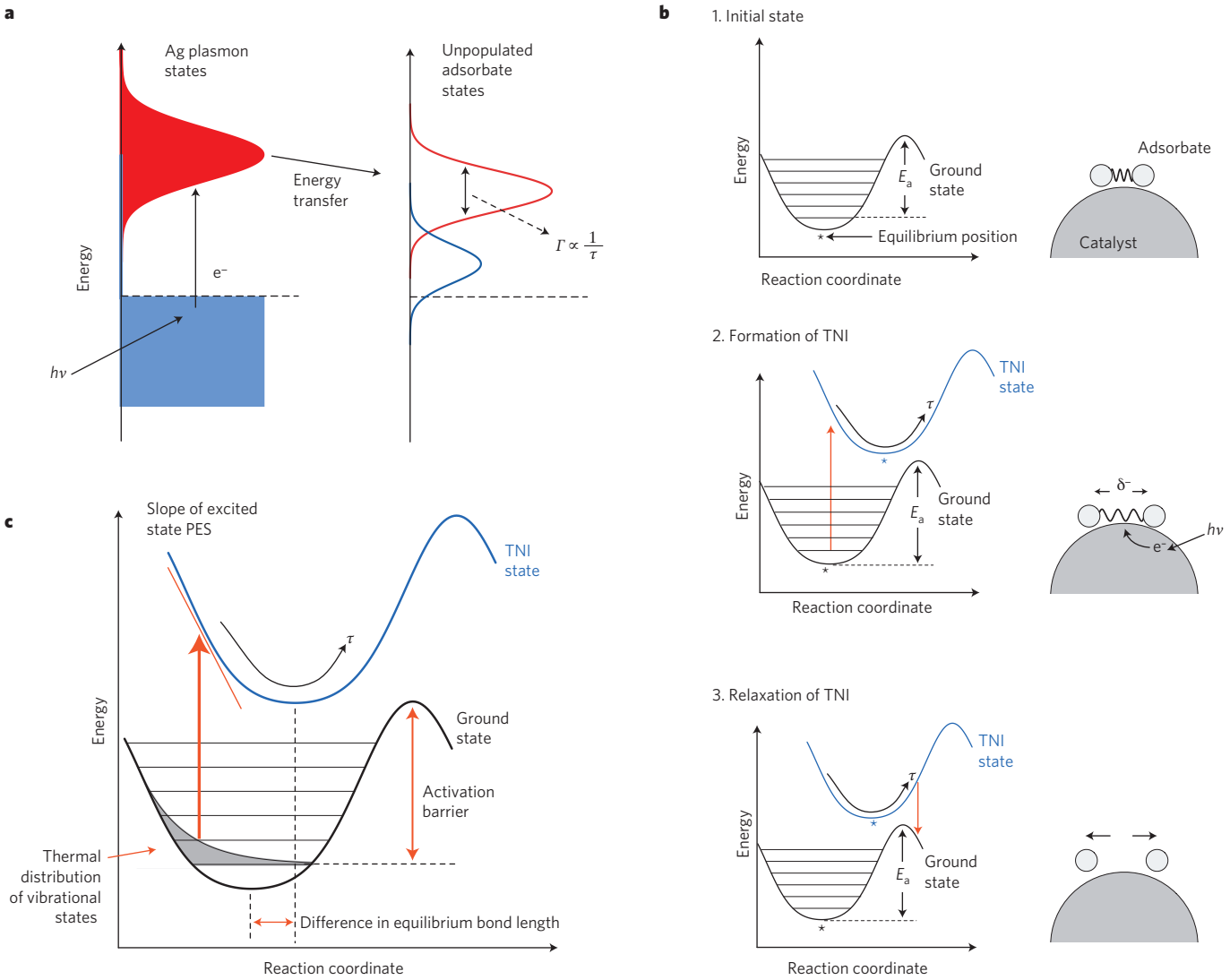

Figure 6 | Mechanism of plasmon photocatalysis on metals. a, Schematic of energy transfer from photo-excited plasmon states to unpopulated adsorbate states. The excited plasmon states interact through an electron-scattering process with unpopulated adsorbate levels. **b**, Proposed mechanism for electron-induced oxygen dissociation on a photo-excited plasmonic metal. 1. The adsorbate is initially on its ground-state potential energy surface. E_a is defined as the activation barrier for dissociation. 2. The electron-scattering process produces a TNI (δ^-). The adsorbate travels on the TNI potential energy surface, gaining kinetic energy along the reaction coordinate. 3. After a short lifetime, τ, the electron decays back to the metal Fermi level and the adsorbate returns to the ground-state potential energy surface with increased vibrational energy. If the energy transfer is sufficient to overcome E_a, the reaction will occur. **c**, The efficiency of the scattering processes for inducing a catalytic reaction depends on E_a, the thermal population of adsorbate vibrational states, the magnitude of the difference in equilibrium position of the neutral and TNI potential energy surfaces, the slope of the TNI potential energy surface (PES) and τ (ref. 79)

This limited set of experiments performed so far also showed that the distinctive feature of gas-phase photocatalysis on metals that separates these from semiconductors was that higher temperatures led to higher rates of photocatalytic reactions, suggesting that plasmonic nanostructures can efficiently couple photon flux and thermal energy sources to drive chemical transformations. We note that owing to negative relationships between temperature and the lifetime of excited charge carriers, most reactions on semiconductors exhibit inverse dependence on the reaction rates on temperature[85]. The models developed so far for photocatalytic reactions on metal surfaces, mainly based on DIET and DIMET mechanisms, suggest that the capacity of plasmonic metals to couple different external stimuli to drive catalytic transformations is a consequence of a number of factors including: (1) temperature-dependent distribution of excited vibrational states, which significantly affects the probability for the SPR-mediated formation of TNI (the probability for electron transfer into available orbitals), and the probability that the TNI will gain sufficient energy to overcome the reaction barrier; and (2) even more importantly, much lower activation barriers for chemical transformations on metals as opposed to semiconductors allow for significantly lower adsorbate energy required to overcome the activation barrier. This is the main reason why fairly short-lived TNI on metals (on the order of a few femtoseconds) can induce chemical transformations.

Another very unique feature of plasmonic metallic nanostructures that separates these from any other class of materials and allows them to achieve relatively high photocatalytic reaction rates is that they effectively couple the light-harvesting and catalytic function in one material. In contrast, owing to the lack of electron density at the Fermi level[86–88], materials that absorb UV–vis light, such as semiconductors, generally exhibit poor chemical and catalytic activity. The capacity of plasmonic nanostructures to constructively couple numerous stimuli (the energy of photon flux and the energy delivered by thermally heating the plasmonic materials) and to drive chemical transformations with relatively low activation barriers might open avenues for the development of a new class of photocatalysts for various reactions.

Although the studies discussed in this Review showed that SPR is responsible for the transfer of energetic electrons to adsorbates, further analysis is required to address whether this process is mediated by the formation of energetic electrons on the metal surface and their subsequent transfer to the adsorbate, or is a consequence of the direct interaction of surface plasmons with adsorbates. Furthermore, it is not clear whether the plasmon-induced electron transfer to available adsorbate states is a resonant process, or is mediated by electron relaxation, which results in high electronic temperature where only electrons in the high-energy tail of the Fermi–Dirac distribution interact with the adsorbate states. Finally, it is also important to note that the interaction of excited plasmons with adsorbates will be affected by the spatially non-homogeneous distribution of plasmons on the surface of nanostructures. In this regard, hot spots might play a critical role.

Conclusions and outlook

The studies performed so far illustrate that plasmonic metallic nanostructures represent a class of promising materials that can play a role in the conversion of abundant solar energy into chemical energy. From our perspective, the ability of plasmonic nanostructures to concentrate UV–vis radiation in small volumes might prove to be the most critical for possible use of these building blocks in the design of composite photocatalysts for the production of solar fuels. This feature of plasmonic nanostructures allows for a selective amplification of the intensity of an electromagnetic source (such as sunlight, which is very diffuse) in the regions of the composite photocatalyst where photocatalytic reactions are taking place (that is, the semiconductor/liquid interface). Also, by manipulating the resonant wavelength, by changing the size and shape of plasmonic nanostructures, it is possible to use the entire solar spectrum and to extend the absorption band of composite photocatalysts to the regions that might be inaccessible to the semiconductor. This characteristic of plasmonic nanostructures also permits very direct and efficient channelling of energetic electrons into adsorbates, accelerating chemical reactions on the surface of the metallic nanostructure.

Recent examples have shed light on many factors that play a role in SPR-mediated chemical transformations on semiconductors and metals, but predictive models that can quantify the interplay between different factors that affect the overall performance and guide the design of highly efficient materials need to be developed. Without such comprehensive predictive models it is impossible to discuss the upper limits of SPR-induced enhancements in the rates of photocatalytic reactions on semiconductors and plasmonic nanostructures, or to identify the geometries of composite photocatalysts that could achieve these limits. Any practically useful predictive model needs to capture the elementary chemical steps involved in a photocatalytic transformation, the relationships between the geometry of building blocks and the rates of formation of energetic charge carriers, as well as the dynamics of excited and neutral molecular states. Recent progress in first-principles analysis of surface chemical transformations on metals and semiconductors using quantum chemical approaches (for example, density functional theory and time-dependent density functional theory), and the development of simulation techniques that accurately predict the near- and far-field optical properties of complex systems (such as the methods of finite-difference time domain (FDTD) and discrete dipole approximation) represent a reasonable foundation for these models.

Even without the predictive models, it is clear that to take full advantage of the plasmonic nanostructures we need to master not only the design and synthesis of individual building blocks (that is, composition, size and shape of nanostructures) but also the nanoscale assembly of these blocks into targeted three-dimensional structures (that is, hot-spot engineering), where plasmonic metal and semiconductor building blocks are positioned precisely with respect to each other. Various concepts recently advanced in the field of directed assembly on the nanoscale may prove to be useful in the design of optimal three-dimensional structures[89]. Furthermore, major advancements are needed in the area of reactor engineering for photochemical processes, where optimal reactor geometries and designs that allow for the efficient use of solar flux need to be developed.

It is reasonable to assume that with the significant contemporary focus on this field, the next few years will bring major advancements in all three areas: the development of robust predictive models, new synthetic strategies that would allow for the design of targeted composite photocatalysts, and new reactor designs.

References

1. El-Sayed, M. A. Some interesting properties of metals confined in time and nanometer space of different shapes. *Acc. Chem. Res.* **34,** 257–264 (2001).
2. Burda, C., Chen, X., Narayanan, R. & El-Sayed, M. A. Chemistry and properties of nanocrystals of different shapes. *Chem. Rev.* **105,** 1025–1102 (2005).
3. Kelly, K. L., Coronado, E., Zhao, L. L. & Schatz, G. C. The optical properties of metal nanoparticles: The influence of size, shape, and dielectric environment. *J. Phys. Chem. B* **107,** 668–677 (2003).
4. Brus, L. Noble metal nanocrystals: Plasmon electron transfer photochemistry and single-molecule Raman spectroscopy. *Acc. Chem. Res.* **41,** 1742–1749 (2008).
5. Rycenga, M. *et al.* Controlling the synthesis and assembly of silver nanostructures for plasmonic applications. *Chem. Rev.* **111,** 3669–3712 (2011).
6. Xia, Y., Xiong, Y., Lim, B. & Skrabalak, S. E. Shape-controlled synthesis of metal nanocrystals: Simple chemistry meets complex physics? *Angew. Chem. Int. Ed.* **48,** 60–103 (2009).
7. Jiang, J., Bosnick, K., Maillard, M. & Brus, L. Single molecule Raman spectroscopy at the junctions of large Ag nanocrystals. *J. Phys. Chem. B* **107,** 9964–9972 (2003).

8. Gunnarsson, L. *et al.* Confined plasmons in nanofabricated single silver particle pairs: Experimental observations of strong interparticle interactions. *J. Phys. Chem. B* **109,** 1079–1087 (2005).
9. Evanoff, D. D. & Chumanov, G. Synthesis and optical properties of silver nanoparticles and arrays. *ChemPhysChem* **6,** 1221–1231 (2005).
10. Kamat, P. V. Photophysical, photochemical and photocatalytic aspects of metal nanoparticles. *J. Phys. Chem. B* **106,** 7729–7744 (2002).
11. Tian, Y. & Tatsuma, T. Mechanisms and applications of plasmon-induced charge separation at TiO_2 films loaded with gold nanoparticles. *J. Am. Chem. Soc.* **127,** 7632–7637 (2005).
12. Jain, P. K., Huang, X., El-Sayed, I. H. & El-Sayed, M. A. Noble metals on the nanoscale: Optical and photothermal properties and some applications in imaging, sensing, biology, and medicine. *Acc. Chem. Res.* **41,** 1578–1586 (2008).
13. Schuller, J. A. *et al.* Plasmonics for extreme light concentration and manipulation. *Nature Mater.* **9,** 193–204 (2010).
14. Nie, S. & Emory, S. R. Probing single molecules and single nanoparticles by surface-enhanced Raman scattering. *Science* **275,** 1102–1106 (1997).
15. Kühn, S., Håkanson, U., Rogobete, L. & Sandoghdar, V. Enhancement of single-molecule fluorescence using a gold nanoparticle as an optical nanoantenna. *Phys. Rev. Lett.* **97,** 017402 (2006).
16. Atwater, H. A. & Polman, A. Plasmonics for improved photovoltaic devices. *Nature Mater.* **9,** 205–213 (2010).
17. Larsson, E. M., Langhammer, C., Zorić, I. & Kasemo, B. Nanoplasmonic probes of catalytic reactions. *Science* **326,** 1091–1094 (2009).
18. Adleman, J. R., Boyd, D. A., Goodwin, D. G. & Psaltis, D. Heterogenous catalysis mediated by plasmon heating. *Nano Lett.* **9,** 4417–4423 (2009).
19. Wei Hsuan Hung, W. H., Aykol, M., Valley, D., Hou, W. & Cronin, S. B. Plasmon resonant enhancement of carbon monoxide catalysis. *Nano Lett.* **10,** 1314–1318 (2010).
20. Takata, T., Tanaka, A., Hara, M., Kondo, J. N. & Domen, K. Recent progress of photocatalysts for overall water splitting. *Catal. Today* **44,** 17–26 (1998).
21. Kudo, A. & Miseki, Y. Heterogeneous photocatalyst materials for water splitting. *Chem. Soc. Rev.* **38,** 253–278 (2009).
22. Fujishima, A. & Honda, K. Electrochemical photolysis of water at a semiconductor electrode. *Nature* **238,** 37–38 (1972).
23. Bard, A. J. & Fox, M. A. Artificial photosynthesis: Solar splitting of water to hydrogen and oxygen. *Acc. Chem. Res.* **28,** 141–145 (1995).
24. Grätzel, M. Photoelectrochemical cells. *Nature* **414,** 338–344 (2001).
25. Walter, M. G. *et al.* Solar water splitting cells. *Chem. Rev.* **110,** 6446–6473 (2010).
26. Cesar, I., Sivula, K., Kay, A., Zboril, R. & Grätzel, M. Influence of feature size, film thickness, and silicon doping on the performance of nanostructured hematite photoanodes for solar water splitting. *J. Phys. Chem. C* **113,** 772–782 (2009).
27. Hou, Y. *et al.* Bioinspired molecular co-catalysts bonded to a silicon photocathode for solar hydrogen evolution. *Nature Mater.* **10,** 434–438 (2011).
28. Maiolo, J. R. III *et al.* High aspect ratio silicon wire array photoelectrochemical cells. *J. Am. Chem. Soc.* **129,** 12346–12347 (2007).
29. Goldberger, J. *et al.* Single-crystal gallium nitride nanotubes. *Nature* **422,** 599–602 (2003).
30. Subramanian, V., Wolf, E. E. & Kamat, P. V. Semiconductor–metal composite nanostructures. To what extent do metal nanoparticles improve the photocatalysic activity of TiO_2 films? *J. Phys. Chem. B* **105,** 11439–11446 (2001).
31. Subramanian, V., Wolf, E. E. & Kamat, P. V. Catalysis with TiO_2/gold nanocomposites. Effect of metal particle size on the Fermi level equilibration. *J. Am. Chem. Soc.* **126,** 4943–4950 (2004).
32. Silva, C. G., Juárez, R., Marino, T., Molinari, R. & García, H. Influence of excitation wavelength (UV or visible light) on the photocatalytic activity of titania containing gold nanoparticles for the generation of hydrogen or oxygen from water. *J. Am. Chem. Soc.* **133,** 595–602 (2011).
33. Arabatzis, I. M. *et al.* Silver-modified titanium dioxide thin films for efficient photodegradation of methyl orange. *Appl. Catal. B* **42,** 187–201 (2003).
34. Adams, D. M. *et al.* Charge transfer on the nanoscale: Current status. *J. Phys. Chem. B* **107,** 6668–6697 (2003).
35. Awazu, K. *et al.* Plasmonic photocatalyst consisting of silver nanoparticles embedded in titanium dioxide. *J. Am. Chem. Soc.* **130,** 1676–1680 (2008).
36. Christopher, P., Ingram, D. B. & Linic, S. Enhancing photochemical activity of semiconductor nanoparticles with optically active Ag nanostructures: Photochemistry mediated by Ag surface plasmons. *J. Phys. Chem. C* **19,** 9173–9177 (2010).
37. Zhou, X., Hu, C., Hu, X., Peng, T. & Qu, J. Plasmon-assisted degradation of toxic pollutants with Ag-AgBr/Al_2O_3 under visible-light irradiation. *J. Phys. Chem. C* **114,** 2746–2750 (2010).
38. Kowalska, E., Abe, R. & Ohtani, B. Visible light-induced photocatalytic reaction of gold-modified titanium(iv) oxide particles: action spectrum analysis. *Chem. Comm.*, 241–243 (2009).
39. Kowalska, E., Mahaney, O. O. P., Abe, R. & Ohtani, B. Visible-light-induced photocatalysis through surface plasmon excitation of gold on titania surfaces. *Phys. Chem. Chem. Phys.* **12,** 2344–2355 (2010).
40. Kumar, M. P. *et al.* Field effects in plasmonic photocatalyst by precise SiO_2 thickness control using atomic layer deposition. *ACS Catal.* **1,** 300–308 (2011).
41. Primo, A., Corma, A. & García, H. Titania support gold nanoparticles as photocatalyst. *Phys. Chem. Chem. Phys.* **13,** 886–910 (2011).
42. Zhai, W., Xue, S., Zhu, A., Luo, Y. & Tian, Y. Plasmon-driven selective oxidation of aromatic alcohols to aldehydes in water with recyclable Pt/TiO_2 nanocomposites. *ChemCatChem* **3,** 127–130 (2011).
43. Tian, Y. & Tatsuma, T. Plasmon-induced photoelectrochemistry at metal nanoparticles supported on nanoporous TiO_2. *Chem. Comm.*, 1810–1811 (2004).
44. Ingram, D. B. & Linic, S. Water splitting on composite plasmonic-metal/semiconductor photoelectrodes: Evidence for selective plasmon-induced formation of charge carriers near the semiconductor surface. *J. Am. Chem. Soc.* **133,** 5202–5205 (2011).
45. Chen, J-J., Wu, J. C. S., Wu, P. C. & Tsai, D. P. Plasmonic photocatalyst for H_2 evolution in photocatalytic water splitting. *J. Phys. Chem. C* **115,** 210–216 (2011).
46. Thimsen, E., Le Formal, F., Grätzel, M. & Warren, S. C. Influence of plasmonic Au nanoparticles on the photoactivity of Fe_2O_3 electrodes for water splitting. *Nano Lett.* **11,** 35–43 (2011).
47. Liu, Z., Hou, W., Pavaskar, P., Aykol, M. & Cronin, S. B. Plasmon resonant enhancement of photocatalytic water splitting under visible illumination. *Nano Lett.* **11,** 1111–1116 (2011).
48. Primo, A., Marino, T., Corma, A., Molinari, R. & García, H. Efficient visible-light photocatalytic water splitting by minute amounts of gold supported on nanoparticulate CeO_2 obtained by a biopolymer templating method. *J. Am. Chem. Soc.* **133,** 6930–6933 (2011).
49. Youngblood, W. J. *et al.* Photoassisted overall water splitting in a visible light-absorbing dye-sensitized photoelectrochemical cell. *J. Am. Chem. Soc.* **131,** 926–927 (2009).
50. Jain, P. K., Lee, K. S., El-Sayed, I. H. & El-Sayed, M. A. Calculated absorption and scattering properties of gold nanoparticles of different size, shape, and composition: Applications in biological imaging and biomedicine. *J. Phys. Chem. B*, **110,** 7238–7248 (2006).
51. Lee, J. *et al.* Bioconjugated Ag nanoparticles and CdTe nanowires: Metamaterials with field-enhanced light absorption. *Angew. Chem. Int. Ed.* **45,** 4819–4823 (2006).
52. Anger, P., Bharadwaj, P. & Novotny, L. Enhancement and quenching of single-molecule fluorescence. *Phys. Rev. Lett.* **96,** 113002-1-4 (2006).
53. Yates, Jr., J. T. Photochemistry on TiO_2: Mechanisms behind the surface chemistry. *Surf. Sci.* **603,** 1605–1612 (2009).
54. Zhang, Z. & Yates, Jr., J. T. Direct observation of surface-mediated electron–hole pair recombination in TiO_2(110). *J. Phys. Chem. C* **114,** 3098–3101 (2010).
55. Kulkarni, A. P., Noone, K. M., Munechika, K., Guyer, S. R. & Ginger, D. S. Plasmon-enhanced charge carrier generation in organic photovoltaic films using silver nanoprisms. *Nano Lett.* **10,** 1501– 1505 (2010).
56. Lee, J., Govorov, A. O., Dulka, J. & Kotov, N. A. Bioconjugates of CdTe nanowires and Au nanoparticles: Plasmon-exciton interactions, luminescence enhancement, and collective effects. *Nano Lett.* **4,** 2323–2330 (2004).
57. Ingram, D. B., Christopher, P., Bauer, J. L. & Linic, S. Predictive model for the design of plasmonic metal/semiconductor composite photocatalysts. *ACS Catal.* **1,** 1441–1447 (2011).
58. Wolkow, R. A. & Moskovits, M. Enhanced photochemistry on silver surfaces. *J. Chem. Phys.* **87,** 5858–5869 (1987).
59. Lee, J., Govorov, A. O. & Kotov, N. A. Nanoparticle assemblies with molecular springs: A nanoscale thermometer. *Angew. Chem. Int. Ed.* **44,** 7439–7442 (2005).
60. Govorov, A. O., Lee, J. & Kotov, N. A. Theory of plasmon-enhanced Förster energy transfer in optically excited semiconductor and metal nanoparticles. *Phys. Rev. B* **76,** 125308 (2007).
61. Van Der Meer, B. W., Coker, G. & Chen, S. Y. S. *Resonance Energy Transfer: Theory and Data* (Wiley, 1994).
62. Ho., W. Reactions at metal surfaces induced by femtosecond lasers, tunneling electrons and heating. *J. Phys. Chem.* **100,** 13050–13060 (1996).
63. White, J. M., Using photons and electrons to drive surface chemical reactions. *J. Mol. Catal. A* **131,** 71–90 (1998).
64. Watanabe, K., Menzel, D., Nilius, N. & Freund, H-J. Photochemistry of metal nanoparticles. *Chem. Rev.* **106,** 4301–4320 (2006).
65. Hatch, S. R., Zhu, X-Y., White, J. M. & Campion, A. Photoinduced pathways to dissociation and desorption of dioxygen on Ag(110) and Pt(111). *J. Phys Chem.* **95,** 1759–1768 (1991).
66. So, S. K., Franchy, R. & Ho, W. Photodesorption of NO from Ag(111) and Cu(111). *J. Chem. Phys.* **95,** 1385–1399 (1991).
67. Mieher, W. D. & Ho., W. Bimolecular surface photochemistry: mechanisms of CO oxidation on Pt(111) at 85 K. *J. Chem. Phys.* **99,** 9279–9295 (1993).
68. Zhu, H., Ke, X., Yang, X., Sarina, S. & Liu, H. Reduction of Nitroaromatic compounds on supported gold nanoparticles by visible and ultraviolet light. *Angew. Chemie. Int. Ed.* **49,** 9657–9661 (2010).

69. Navalon, S., de Miguel, M., Martin, R., Alvaro, M. & Garcia, H. Enhancement of the catalytic activity of supported gold nanoparticles for the Fenton reaction by light. *J. Am. Chem. Soc.* **133,** 2218–2226 (2011).
70. Christopher, P., Xin, H. & Linic, S. Visible light enhanced catalytic oxidation reactions on plasmonic Ag nanostructures. *Nature Chem.* **3,** 467–472 (2011).
71. Chen, X., Zhu, H-Y., Zhao, J-C., Zheng, Z-F. & Gao, X-P. Visible-light-driven oxidation of organic contaminants in air with gold nanoparticle catalysts on oxide supports. *Angew. Chemie. Int. Ed.* **47,** 5353–5356 (2008).
72. Zhu, H., et. al. Mechanism of supported gold nanoparticles as photocatalysts under ultraviolet and visible irradiation. *Chem. Comm,* 7524–7526 (2010).
73. Chen, X., et. al. Supported silver particles as photocatalysts under ultraviolet and visible light irradiation. *Green Chem.* **12,** 414–419 (2010).
74. Busch, D. G. & Ho, W. Direct observation of the crossover from single to multiple excitations in femtosecond surface photochemistry. *Phys. Rev. Lett.* **77,** 1338–1341 (1996).
75. Bonn, M. *et al.* Phonon-versus electron-mediated desorption and oxidation of CO on Ru(0001). *Science*, **285,** 1042 (1999).
76. Denzler, D. N., Frischkorn, C., Hess, C., Wolf, M. & Ertl, G. Electronic excitation and dynamic promotion of a surface reaction. *Phys. Rev. Lett.*, **91,** 226102 (2003).
77. Buntin, S. A., Richter, L. J., Cavanagh, R. R. & King, D. S. Optically driven surface reaction: evidence for the role of hot electrons. *Phys. Rev. Lett.* **61,** 1321–1325 (1988).
78. Wingreen, N. S., Jacobsen, K. W. & Wilkins, J. W. Inelastic scattering in resonant tunneling. *Phys. Rev. B* **40,** 11834–11850 (1989).
79. Olsen, T., Gavnholt, J. & Schiotz, J. Hot-electron-mediated desorption rates calculated from excited state potential energy surfaces. *Phys. Rev. B* **79,** 035403 (2009).
80. Olsen, T. & Schiotz, J. Origin of power laws for reactions at metal surfaces mediated by hot electrons. *Phys. Rev. Lett.* **103,** 238301 (2009).
81. Gadzuk, J. W., Richter, L. J., Buntin, S. A., King, D. S. & Cavanagh, R. R. Laser-excited hot-electron induced desorption: A theoretical model applied to NO/Pt(111). *Surf. Sci.* **235,** 317–333 (1990).
84. Avouris, P. & Walkup, R. E. Fundamental mechanisms of desorption and fragmentation induced by electronic transitions at surfaces. *Annu. Rev. Phys. Chem.* **40,** 173–206 (1989).
83. Dai, H-L. & Ho, W. *Laser Spectroscopy and Photochemistry on Metal Surfaces* (World Scientific, Singapore, 1995).
84. Gadzuk, J. W. Hot-electron femtochemistry at surfaces: on the role of multiple electron processes in desorption. *Chem. Phys.* **251,** 87–97 (2000).
85. Westrich, T. A., Dahlberg, K. A., Kaviany, M. & Schwank, J. W. High-Temperature Photocatalytic Ethylene Oxidation over TiO_2. *J. Phys. Chem. C*, **115,** 16537–16543 (2011).
86. Hammer, B. & Nørskov, J. K. Why gold is the noblest of all the metals. *Nature*, **376,** 238 (1995).
87. Nikolla, E., Schwank, J. & Linic, S. Measuring and relating the electronic structures of nonmodel supported catalytic materials to their performance. *J. Am. Chem. Soc.* **131,** 2747–2754 (2009).
88. Xin, H. & Linic, S. Exceptions to the *d*-band model of chemisorption on metal surfaces: the dominant role of repulsion between adsorbate states and metal *d*-states. *J. Chem. Phys.* **132,** 221101 (2010).
89. Glotzer, S. C. & Solomon, M. J. Anisotropy of building blocks and their assembly into complex structures. *Nature Mater.* **6,** 557–562 (2007).
90. Nozik, A. J. & Memming, R. Physical chemistry of semiconductor–liquid interfaces. *J. Phys. Chem.* **100,** 13061–13078 (1996).
91. Serpone, N. & Pelizzetti, E. *Photocatalysis* (Wiley, 1989).

Acknowledgements

We gratefully acknowledge support from United States Department of Energy, Office of Basic Energy Science, Division of Chemical Sciences (FG-02-05ER15686) and National Science Foundation (CBET-0966700, CBET-1132777 and CHE-1111770). S.L. acknowledges the DuPont Young Professor grant and the Camille Dreyfus Teacher-Scholar Award from the Camille & Henry Dreyfus Foundation. We also acknowledge H. Xin for discussions and insight.

Additional information

The authors declare no competing financial interests.